

Material Point Method Simulations of Transverse Fracture in Wood with Realistic Morphologies

By J. A. Nairn¹

Wood Science & Engineering, Oregon State University, Corvallis, OR 97331, USA

Keywords

Material point method
Numerical modeling
RT fracture
TR fracture;
Transverse fracture

Summary

A new numerical method called the material point method (MPM) is well suited for modeling problems with complex geometries and with crack propagation in arbitrary directions. In this paper, these features of MPM were used to simulate transverse fracture in solid wood. The simulations were run on the scale of growth rings. The ease of MPM for handling complex geometries was helpful for modeling realistic morphologies of earlywood and latewood. Because MPM discretizes a body into material points, it was possible to go directly from a digital image of wood to a numerical model by assigning location and properties of material points based on intensity or color of pixels in an image. Because the description of cracks in MPM is meshless, it can handle a variety of crack propagation and direction criteria and can simulate complex crack paths that are a consequence of the morphology of the specimen. MPM simulations were run for cracks in the radial direction, the tangential direction, and at two angles to the radial direction. The specimens were loaded by axial displacement or by wedge opening. The MPM simulations fully included contact effects during the wedge loading. Finally, the potential for coupling such simulations to new experiments as a tool for characterization of wood is discussed.

Introduction

Due to anisotropy, the fracture properties of wood depend on crack growth direction. In the nomenclature of wood fracture mechanics, key fracture growth directions are characterized by two letters as RT, RL, TR, TL, LR, or LT. The first letter denotes the normal to the crack plane (radial, tangential, or longitudinal direction) while the second letter denotes the crack propagation direction (Ashby 1985). Because the grain direction is much stronger than other directions, cracks rarely propagate through wood fibers and thus crack planes normal to the longitudinal direction (LR and LT cracks) are rarely observed. The other four directions propagate transverse to wood fibers and are all important when characterizing wood fracture. The RL and TL directions are cracks parallel to the wood grain. The TR and RT directions are cracks propagating in a transverse cross section of wood. RL and TL cracks normally remain in the L direction because deviation would cross wood fibers. In contrast, all crack paths in a transverse cross section of wood are normal to wood fibers and thus can propagate in any direc-

tion without crossing wood fibers. Furthermore, propagation in the radial direction may be different when propagating toward the bark (denoted TR+) then when propagating toward the pith (denoted TR-). Figure 1 illustrates a general nomenclature for transverse fracture of TR+ θ where θ is the angle between the TR+ direction and the propagation direction. In this general nomenclature, TR+ is TR+0, RT is TR \pm 90, and TR- is TR+180. The subject of this paper is numerical simulation of any TR+ θ crack.

Early work on transverse fracture in wood treated it by standard fracture mechanics methods. For example, Attack (1961) measured toughness of green spruce to be 100 J/m² in the TR- direction and 180 J/m² in the RT direction. Ashby (1985) contends that the TR \pm directions should have lower toughness than RT cracks because the TR \pm cracks may find a path along radial ray cells as a potential plane of weakness. This contention agrees with the results of Attack (1961). Others have used fracture mechanics methods for stress intensity factor. For example, Schniewind and Centeno (1973) measured RT and TR stress intensity factors for air-dried Douglas-Fir and found

1. Email: John.Nairn@oregonstate.edu

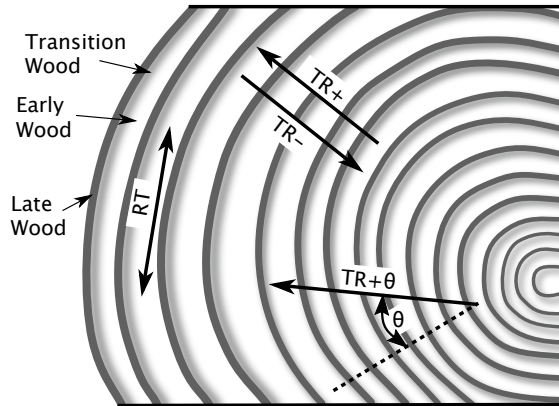


Fig. 1. Definition of directions for transverse crack propagation in solid wood and identification of early wood, transition wood, and late wood. $TR+\theta$ is a generic nomenclature by which the other directions can be labeled: $TR+ = TR+0$, $TR- = TR+180$, and $RT=TR\pm 90$.

them both equal to $0.35 \text{ MPa} \sqrt{\text{m}}$ or no difference between the two transverse directions.

Because a transverse section of wood is not homogeneous, it can be misleading to define a material property for global $TR+\theta$ toughness. Instead, transverse fracture should be recognized as crack growth through a heterogeneous, composite material. The problem should be approached as a composite problem with the toughness properties depending on the morphology of the specimen such as the geometry and properties of earlywood (EW), transition wood, and latewood (LW), and location of the crack within that morphology. The problem should be broken down into properties of the components rather than interpreted as a single global property. For an analogy, it is more appropriate to speak of the toughness of the steel used in a hull of a ship than to speak of the fracture toughness of the ship.

Modeling of composite fracture should begin with observations of failure mechanisms that depend on the structure of the composite (Nairn and Hu 1994). In observations of transverse fracture, Ashby *et al.* (1985) noted that in low density wood, such as balsa or some EW zones, fracture is propagated predominantly by cell wall ruptures, while in higher density wood, including LW zones, tend to fracture by peeling the middle lamellae between cell walls. Dill-Langer *et al.* (2002) observed RT fracture characterized by much cell wall rupture while TR fracture proceeded mainly by cell wall peeling. These authors also looked at $TR+135$ fracture and observed a

zig-zag crack path. Crack growth, particularly during TR fracture, is non-steady. Thuvander and Berglund (2000) described crack arrest as the crack propagated from EW toward LW. At higher load, the crack would jump across the LW. Although crack growth was by cell-wall peeling, the crack plane could shift during jumps across LW. Fruhmann *et al.* (2003) also noted non-stable crack growth as the crack tip moved between EW and LW.

These experimental observations are on two different scales. On a microscopic scale, the observations relate to mechanisms on the cell-wall level. These mechanisms determine the global properties of wood but are not amenable to fracture mechanics modeling. On a growth ring scale, however, a transverse section can be modeled as a composite of EW, transition wood, and LW. On this scale, wood could be considered as a continuum with varying mechanical and fracture properties and crack growth through the structure can be modeled as a continuum, composite fracture problem. Some experimental work has tried to record the effect of local geometry on fracture. Ando *et al.* (1991, 1999) pointed out that toughness may vary with position and attempted to measure K_{Ic} as a function of position. Unfortunately, the authors used equations for extracting K_{Ic} that were based on homogeneous materials and thus they actually recorded an apparent toughness. Better characterization of local properties requires numerical modeling to extract properties from experimental results. Both Ando *et al.* (1999) and Thuvander *et al.* (2000) tried finite element analysis (FEA) of a TR crack spanning EW and LW. These results, however, simplified EW and LW as perfectly straight and parallel layers in a 2D FEA analysis.

This paper describes use of the material point method (MPM) as a tool for modeling transverse crack propagation in wood. Advantages of MPM over the more-common FEA are that it is easy to discretize a realistic morphology for the specimen and it is easy to model crack propagation in arbitrary directions. Simulations were run for $TR+$, $TR-$, RT , $TR+45$, and $TR+135$ fracture and for either tensile or wedge-opening specimens.

The Material Point Method

The material point method (MPM) was developed as a numerical method for solving problems in dynamic solid mechanics, *i.e.*, an alternate ap-

proach, with alternate characteristics, for solving problems traditionally studied by dynamic FEA methods (Sulsky *et al.* 1994; 1995; 1996; Zhou 1998). In MPM, a solid body is discretized into a collection of points much like a computer image is represented by pixels (see Figure 2). As the dynamic analysis proceeds, the solution is tracked on the material points by updating all required properties such as position, velocity, acceleration, stress state, *etc.*. At each time step, the particle information is extrapolated to a background grid that provides a platform for solving the equations of motion and updating all particle properties. The particles interact as a solid through the grid. This combination of Lagrangian (particles) and Eulerian (grid) methods has proven useful for solving solid mechanics problems including those with large deformations or rotations and involving materials with history-dependent properties such as plastic or viscoelastic materials (Sulsky *et al.* 1994). MPM is available in public-domain, 3D, parallel code (Parker 2002) or 2D code (Nairn 2005), is amenable to implicit integration methods (Guilkey and Weiss 2003) and generalized interpolation schemes that optimize accuracy (Bardenhagen and Kober 2004). Although MPM is frequently compared to finite element methods, a revised derivation of MPM (Bardenhagen and Kober 2004) presents it as a Petrov-Galerkin method that has more similarities with other meshless methods (Atluri and Shen 2002). The “meshless” nature of MPM derives from the fact that the body and the solution are described on the particles while the background grid is only used for calculations.

It is both the particle nature and the meshless nature of MPM that recommend it for analysis of transverse fracture of wood. The particle nature makes it easy to digitize realistic morphologies by translating pixels in a digital image into material points. Based on intensities of pixels, a given material point may be assigned to EW, LW, or possibly transition wood. The analysis is limited only by the quality of the image and the presence of sufficient contrast between different components of the material. Although early MPM did not allow cracks (*i.e.*, did not allow displacement discontinuities), MPM has been extended to CRAMP, which signifies cracks in the material point method (Nairn 2003; Guo and Nairn 2004; 2006; Nairn and Guo 2005). Figure 2 shows a crack in a CRAMP analysis. The crack plane is defined by a series of massless particles that translate through the grid along with the material

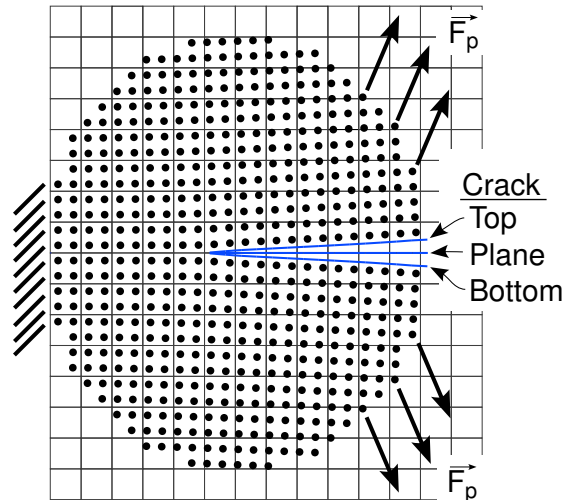


Fig. 2. Sample view of digitization used in MPM and CRAMP. In MPM, the body is digitized into a collection of material points. Boundary conditions may be applied to the grid or directly to particles. In CRAMP, cracks are represented by a series of massless particles. The crack particles track crack-opening displacement that allows for calculation of top and bottom surfaces of the crack.

particles. The crack particles track the local crack opening displacement that provides information for calculation of the top and bottom surfaces of cracks. Knowledge of the local stresses and the crack surfaces is sufficient for calculating fracture mechanics properties for cracks such as J integral and stress intensity factors (Guo and Nairn 2004; 2006).

Simulations that include crack propagation require three steps. First, the stress state and crack-tip parameters are evaluated and it is determined whether or not the stress state is critical for crack growth. If it is determined that the crack should propagate, the crack-tip stress field is then analyzed to determine the direction of propagation. Finally, a new crack particle is added in the selected direction of propagation. A variety of criteria for crack propagation and crack growth direction can be implemented. Unlike FEA analysis of cracks, where cracks must follow mesh lines or there must be time-consuming remeshing, a crack in CRAMP can proceed in arbitrary directions.

All calculations in this paper were done using the open-source, 2D CRAMP code (Nairn 2005). Calculation times ranged from 20 min to several hours when run on a single-processor (1 GHz) computer.

Results

The approach of this modeling was to treat transverse fracture in wood using continuum fracture mechanics with the crack propagating through a complex geometry of EW, transition wood, and LW. In other words, transverse fracture of wood is not a material feature that can be characterized by a single material property, but rather it is a result of a complex interplay of geometry and many material characteristics. The goal of modeling is to understand the effect of geometry and to determine the key material properties. The key properties relevant to crack growth are listed below. Each of them is followed by the assumptions used in these simulations.

Mechanical properties. A transverse section of wood is composed of EW, LW, and transition wood. These zones will have different mechanical properties because their cellular structures will differ. Furthermore, the mechanical properties will depend on moisture content, may be elastic or may exhibit plastic or viscoelastic behavior. A common assumption in wood mechanics is that the properties are isotropic in the transverse plane. Experimental results, however, show that the radial and tangential directions differ with the radial direction being stiffer than the tangential direction (Bodig and Jayne 1982). The radial and tangential directions in EW, transition wood, and LW may differ as well. Finally, transition wood may have a gradient in mechanical properties as the density makes its transition from EW to LW.

Mechanical property assumptions. It was assumed that EW and LW are isotropic and elastic. Since there are no direct experimental results for mechanical properties of pure EW or LW (there are recent results on using digital imaging to extract mechanical properties as a function of position in a large specimen (Jernkvist and Thuvander 2001)), these calculations assumed "reasonable" values of $E = 40$ MPa and $\nu = 0.33$ for EW. The LW properties were set to $E = 1200$ MPa and $\nu = 0.33$. The ratio of 30 was estimated by assuming a density ratio of 3 between LW and EW and the theoretical result that transverse modulus scales as $\rho^3 \approx 27$ (Gibson and Ashby 1997). This modeling included only EW and LW and ignored transition wood; thus no properties or gradient in properties were needed for the latter.

Geometry. There can be much scatter in experimental work on wood, which is caused not only by statistical variations in measurements, but also by actual variations due to specimens having

different morphologies. Common analysis methods for interpreting experiments that idealize the morphology provide no basis for judging effects of morphology. For example, cellular materials, including wood, are often represented as a perfect hexagonal structure (Gibson and Ashby 1997). Some prior modeling of EW and LW represented them as perfectly parallel and straight layers (Ando *et al.* 1999; Thuvander *et al.* 2000). A better approach in analysis is for the geometry in the model to more closely match the morphology of the actual specimens.

Geometry Assumptions. An advantage of MPM is that it is easy to discretize realistic morphologies. For example, Figure 3a shows a digital image Scots pine. An MPM analysis can proceed by examining the intensity of each pixel and translating it to a material point of either EW or LW. If the resolution of the image is higher than the numerical model, the process can average a range of pixels. For the image in Figure 3a, EW or LW were assigned to light or dark pixels, respectively. The resulting MPM model is in Figure 3b. This process is limited only by resolution of the image and by having sufficient contrast between the key morphological features.

Toughness properties. As the crack grows, it will move between different types of wood. A good model should be able to account for variations in toughness depending on local crack tip environment.

Toughness Property Assumptions. In these calculations, the material was assumed to have a constant toughness defined in terms of a critical energy release rate of $G_c = 100$ J/m². This assumption was based on observations that TR fracture proceeds predominantly by cell-wall peeling and thus might be expected to be similar in EW and LW (Thuvander and Berglund 2000; Dill-Langer *et al.* 2002). Certainly, there is no guarantee that toughness remains constant, even if the entire crack growth is by cell-wall peeling. Currently, however, there is no experimental basis for selecting an actual toughness; one approach to measuring local toughness is discussed below. The constant-toughness assumption means that any effects observed in these simulations were due to morphology and to variations in modulus. Experimental observations of RT fracture indicate cell-wall rupture in EW. It is likely that accounting for toughness variations is more important for simulating RT fracture than for TR fracture.

Crack Propagation Criterion. Because realistic morphologies will lead to complicated and vary-

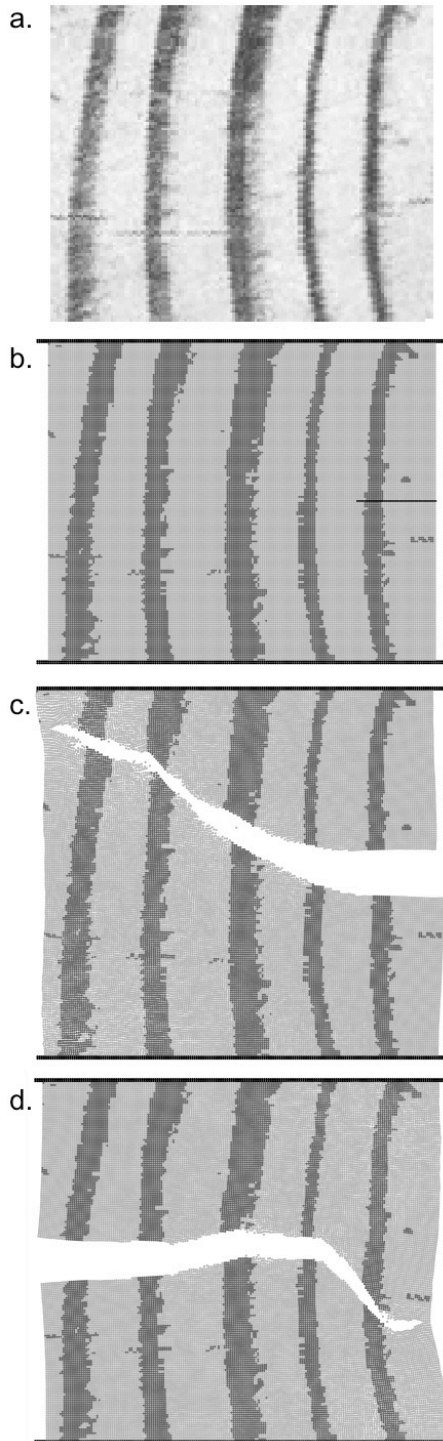


Fig. 3. a. Digitized image of a transverse plane of Scots pine. B. MPM model of the specimen in a. Light areas are early wood and dark areas are late wood. The black lines on top and bottom are the loading grips. The black line in the middle of the right edge is an initial TR+ crack. c. Simulated TR+ crack growth in Scots Pine under uniform axial load. d. Simulated TR- crack growth in Scots Pine under uniform axial load.

ing stress states, the model needs general criteria for predicting whether and in which direction a crack will propagate. Fortunately, MPM is amenable to implementation of a variety of failure criteria.

Crack Propagation Criterion Assumptions.

The conditions for propagation of a crack were based on energy release rate, which was calculated in MPM by the J -integral method (Guo and Nairn 2004). The J integral was converted to energy release rate, G , and the crack was determined to propagate whenever $G > G_c$. The crack growth direction was assumed to be in the principle direction of the deformation field of the crack tip as illustrated in Figure 4. The “Initial Crack” shows a closed crack before application of load and the dot represents two initially aligned reference points on opposite surfaces of the crack located a small distance from the crack tip. The “Propagating Crack” shows the same crack opened and ready to extend. The two dots will displace and the vector $\bar{\delta}$ shows the magnitude and direction of the crack opening displacement field. In these simulations, the crack was assumed to propagate normal to the crack-opening displacement as illustrated by the vector $\Delta\bar{a}$ in Figure 4. For a specimen with a perfect geometry, such as a TR crack with parallel and straight growth rings (Ando *et al.* 1999; Thuvander *et al.* 2000), the crack-opening displacement would always be normal to the original crack, *i.e.*, the crack would always propagate straight. For realistic morphologies or for cracks not aligned with the growth rings, the local geometry and mechanical properties will perturb the crack opening displacement field resulting in curved crack paths.

Once all key model parameters are set, the simulation process proceeds as follows:

1. First, observe a fracture specimen in a microscope and digitize the image with sufficient contrast to resolve EW and LW zones. The author’s software (Nairn 2005) requires the image to be converted to a gray scale BMP file (*e.g.*, Figure 3a).
2. Next, the image is input to MPM software (Nairn 2005). The pixels of the image are scanned and based on intensity, converted into material points for either EW or LW material with specified properties. An MPM model with 33,648 material points (points not resolved in the figure) for the Scots pine image in Figure 3a is shown in Figure 3b.

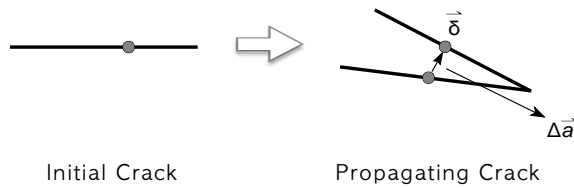


Fig. 4. The left side shows an initial crack with the crack faces closed and a reference point near the crack tip. The right side shows an opened crack under stress. The vector between the reference points is the crack-opening displacement vector. The cracks were assumed to propagate perpendicular to the crack opening displacement vector.

3. The next steps are to introduce a crack and to apply boundary conditions for loading the specimen. Figure 3b shows rigid grips on the top and bottom of the specimen to apply uniform axial displacement at a constant strain rate. The black line in the center is an initial crack for simulation of TR+ crack growth. Most simulations displaced the specimens at 10 m s^{-1} . One set of simulations varied the displacement rate from 2 m s^{-1} to 20 m s^{-1} . High displacement rates were used because the time steps required for the explicit dynamic analysis were small. Although the rates are high, the response was judged to be quasi-static by lack of vibrations in the force-displacement curves prior to crack growth.
4. Finally, the simulation is run, the stresses evolve, and the crack propagates according to conditions assumed in the crack growth and direction criteria.

Figures 3c, 5, and 6 show the results of TR+ crack growth simulations. The crack propagates

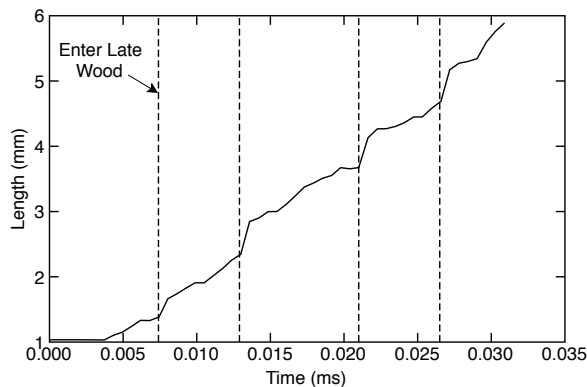


Fig. 5. Crack length vs. time for simulated TR+ crack growth in Scots Pine. The dashed lines are the times the crack tip enters a late wood zone.

across the specimen and changes direction (see Figure 3c). Inspection of the results reveals that as the crack approaches the LW, it diverts toward the thicker, and therefore stiffer, region of the LW zone. Figure 5 shows crack length as a function of time; the slope of this plot is the crack velocity. The dashed lines indicate the time the crack enters each of the four LW zones in the crack path. In agreement with experiments (Thuvander and Berglund 2000), the simulated crack slows down in the EW and speeds up through the LW. Figure 6 shows the average stress-displacement plot for four different displacement rates from 2 m s^{-1} to 20 m s^{-1} . Prior to crack growth, the results are independent of crack speed. After crack initiation at the first peak in stress, all results showed load increases and decreases that corresponded to transit through LW regions. The crack paths were similar for displacement rates 10 m s^{-1} or lower, but changed at the highest rate of 20 m s^{-1} . There are likely two sources for the discrepancies. Because the assumed material properties had no time dependence, a physical reason for displacement rate effect could only be inertial effects. These effects arise at higher speeds and may be the reason the 20 m s^{-1} results differed the most and had a different crack path. Based on observations of results, the results at lower speeds (10 m s^{-1} and lower) should approximate quasi-static conditions. The discrepancies here are likely to be numerical issues associated with material points crossing background cell boundaries that can perturb MPM results at large displacements (Bardenhagen and Kober 2004). These cell-crossing artifacts can be eliminated by using recently-developed generalized interpolation methods

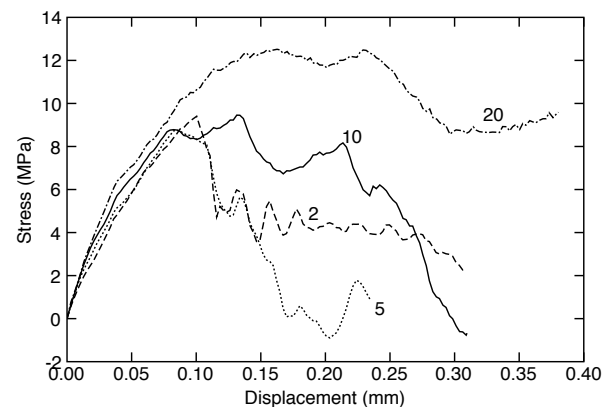


Fig. 6. Average axial stress as a function of displacement for TR+ crack growth at various displacement rates ($2, 5, 10, \text{ and } 20 \text{ m s}^{-1}$).

(Bardenhagen and Kober 2004). Those methods were not available in the code used for this study.

Numerous additional fracture simulations are possible. Figure 3d shows TR- fracture. The crack path was not simply a mirror image of TR+ crack growth indicating that TR+ and TR- fracture properties are different. The differences here were a consequence of the curvatures of the growth rings and their effect on stress state as a crack approaches each ring from the inside or from the outside. Figure 7a shows simulated RT crack growth with the initial crack starting in the LW. The crack remained in the LW throughout loading. A simulation starting in the EW exhibited a crack that was attracted to the LW and thus propagated through LW into the next EW zone resulting in a zig-zag crack path. Figure 7b shows a simulated TR+135 crack; analogous results for a TR+45 crack are not shown. These angled cracks followed zig-zag paths that changed direction as they moved between growth rings. Similar zig-zag paths for TR+135 crack growth have been observed experimentally (Dill-Langer *et al.* 2002).

Fruhmann *et al.* (2003) used a wedge-loading apparatus designed specifically for wood fracture experiments (Stanzl-Tschegg *et al.* 1995). In brief, a specimen is cut with a notch and having angled sides approaching the notch. The angled sides are loaded with frictionless bearings to wedge open the crack while the opposite end of the sample is restrained from movement by a pin. This entire specimen, including the wedge and contact effects, was simulated in MPM. Another feature of MPM is that it can handle contact between two different materials in a more direct manner than modeling contact in FEA (Bardenhagen *et al.* 2001). The bearings and the restraining pin were modeled as steel wheels that contact the specimen through frictionless sliding. In experiments, the wheels rotate on bearings to approximate frictionless conditions. The simulated crack path is presented in Figure 7c. The crack in the wedge-loaded specimen grew in a straighter path than the specimens loaded by uniform axial displacement. The straighter path is a consequence of the bending loads present in wedge loading that are not present during uniform tensile loads. The force-displacement curve had load peaks and drops analogous to those observed in experiments (Fruhmann *et al.* 2003).

These simulations made two assumptions that are likely to be oversimplifications. First, EW and LW were assumed to be isotropic rather than

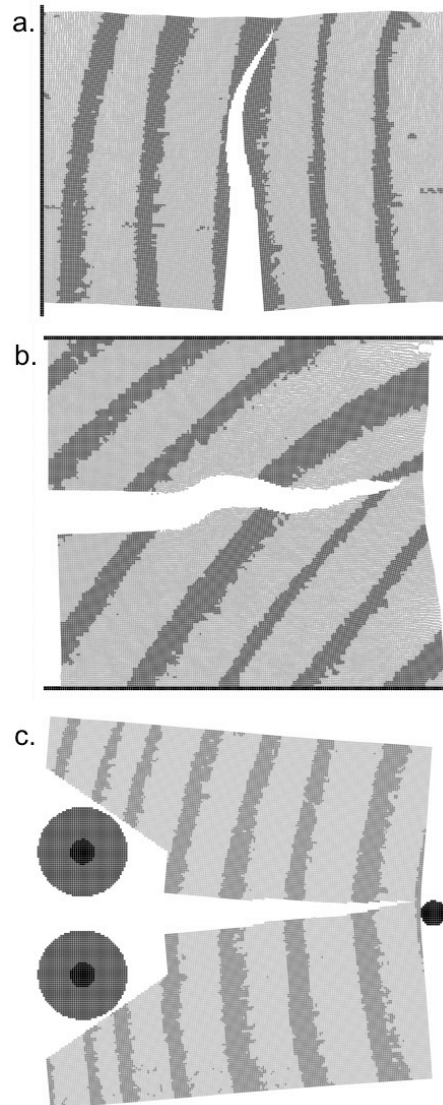


Fig. 7. a. Simulated RT crack growth under uniform horizontal loading when the crack starts in a late wood zone. b. Simulated TR+135 crack growth under uniform axial loading showing a zig-zag crack path. c. Simulated, mode I, TR- crack growth with an explicit model of a splitting device (Stanzl-Tschegg *et al.* 1995). The dark circles are steel wheels for wedging the crack open and a steel pin for restraining the specimen. Contact between the wheels and the specimen was frictionless.

allowing for different properties in the radial and tangential directions. The problem with relaxing this assumption is the difficulty in assigning the radial and tangential direction of each material point. A digital image can identify EW and LW but it does not identify local orientation. One solution may come for “directional filters,” now under development, that process an image and

change color or intensity to reflect orientation (Norell *et al.* 2006). It would be simple to modify MPM software to input two digital images – the original image would locate EW and LW; the filtered image would define orientation of each material point. Even when EW, LW, and orientation are all identified, the simulations still require input of all mechanical properties. Some recent work using digital imaging correlation has potential for extracting variations in mechanical properties between EW and LW in a single specimen (Jernkvist and Thuvander 2001).

The second oversimplification was the assumption of constant toughness. One reason for this assumption was that there are no results for variations in true toughness between EW and LW. A motivation behind simulations is to address this problem by coupling fracture experiments to simulations on models with the same morphology as the actual specimens. If the simulations can model crack growth as a function of time by varying local toughness, it might be possible to extract EW and LW toughness by inverse methods. One complication is dealing with additional uncertainty about crack propagation direction. The wedge-loaded specimen might be useful for separating determination of variations in toughness from effects causing variations in crack direction. Since crack paths during wedge loading are nearly straight, those experiments could be used to determine toughness variations without the need to understand propagation direction. Once the toughness variations are known, a tensile loading geometry could be used to study the criteria for propagation direction.

Conclusions

The simulation results showed that MPM is capable of detailed simulations of fracture in complex materials such as the simulation of transverse fracture in wood. The method is capable of accounting for realistic morphologies, such as the arrangement of growth rings in a specific specimen, and is capable of modeling crack paths in arbitrary directions. Several simplifying assumptions were used for these initial simulations, but there is a clear path for development of MPM into a useful tool for in-depth study of wood fracture.

Neither simulations nor experiments on wood fracture can proceed substantially further alone. Experimental results are available, but it is diffi-

cult to interpret the results in other than simplified global terms. The simulations have been demonstrated, but the calculations depend on many parameters and unknown material properties. The preferred approach is to directly couple experiments and simulations. In other words, specimens are selected, prepared, and imaged. The specimens are then tested experimentally and the images are used in simulations. The goal would be use simulations to interpret experiments. Wherever possible, variations in key parameters could be compared to experiments as a tool for extracting values for those parameters from experimental results. The approach would be computer intensive, but the MPM simulations were efficient.

Acknowledgments

This work was supported by the University of Utah Center for the Simulation of Accidental Fires and Explosions (C-SAFE), funded by the Department of Energy, Lawrence Livermore National Laboratory, under Subcontract B341493 and by the Richardson Family Endowment for Wood Science and Forest Products.

References

- Ando, K., Sato, K., Fushitani, M. (1991) Fracture toughness and acoustic emission characteristics of wood - I: Effects of location of a crack tip in an annual ring. *Mokuzai Gakkaishi* 37:1129-1134
- Ando, K., Ohta, M. (1999) Variability of fracture toughness by the crack tip position in an annual ring of coniferous wood. *Journal of Wood Science* 45:275-283
- Atluri, S. N., Shen, S. (2002) The meshless local Petrov Galerkin (MLPG) method: A simple & less-costly alternative to the finite element and boundary element methods. *Computer Modeling in Engineering & Sciences* 3:11-52
- Attack, D., May, W. D., Morris, E. L., Sproule, R. N. (1961) The energy of tensile and cleavage fracture of black spruce. *Tappi* 8:555-567
- Ashby, M. F., Easterling, K. E., Harrysson, R., Maiti, S. K. (1985) The fracture toughness of woods. *Proceedings of The Royal Society of London, Series A: Mathematical and Physical Sciences* 398:261-280
- Bardenhagen, S. G., Guilkey, J. E., Roessig, K. M., Brackbill, J. U., Witzel, W. M., Foster, J. C. (2001) An improved contact algorithm for the material point method and application to stress propagation in granular material. *Computer Modeling in Engineering & Sciences* 2:509-522

- Bardenhagen, S. G., Kober, E. M. (2004) The generalized interpolation material point method. *Computer Modeling in Engineering & Sciences* 5:477-496
- Bodig, J., Jayne, B. A. *Mechanics of Wood and Wood Composites*. Van Nostran-Reinhold Co, Inc., New York, 1982.
- Dill-Langer, G., Lutze, S., Aicher, S. (2002) Microfracture in wood monitored by confocal laser scanning microscopy. *Wood Science and Technology* 36:487-499
- Fruhmann, K., Burgert, I., Stanzl-Tschegg, S. E., Tschegg, E. K. (2003) Mode I fracture behaviour on the growth ring scale and cellular level of spruce (*picea abies* [L.] Karst.) and beech (*fagus sylvatica* L.) loaded in the TR crack propagation system. *Holzforschung* 57:653-660
- Gibson, L. J., Ashby, M. F. *Cellular Solids: Structure and Properties*. Cambridge University Press, Cambridge, England, 1997
- Guilkey, J. E., Weiss, J. A. (2003) Implicit time integration for the material point method: Quantitative and algorithmic comparisons with the finite element method. *Int. J. Num. Meth. Engng.*, 57:1323-1338
- Guo, Y., Nairn, J. A. (2004) Calculation of J-integral and stress intensity factors using the material point method. *Computer Modeling in Engineering & Sciences* 6:295-308
- Guo, Y., Nairn, J. A. (2006) Three-dimensional dynamic fracture analysis in the material point method. *Computer Modeling in Engineering & Sciences*, in press
- Jernkvist, L.O., Thuvander, F. (2001) Experimental determination of stiffness variation across growth rings in *picea abies*. *Holzforschung* 55:309-317
- Nairn, J. A., Hu, S. (1994) Micromechanics of damage: A case study of matrix microcracking, in *Damage Mechanics of Composite Materials*, editor: Talreja, R., Elsevier, Amsterdam, 187-243.
- Nairn, J. A. (2003) Material point method calculations with explicit cracks. *Computer Modeling in Engineering & Sciences*, 4:649-664
- Nairn, J. A. (2005) Source code and documentation for N a i r n M P M M P M s o f t w a r e . <http://oregonstate.edu/~nairmj/>
- Nairn, J. A., Guo, Y. (2005) Material point method calculations with explicit cracks, fracture parameters, and crack propagation. In 11th Int. Conf. Fracture, Turin, Italy, Mar 20-25, 2005.
- Norell, K., Borgefors, G., Bengsston, E. (2006) Personal communication.
- Parker, S. G. (2002) A component-based architecture for parallel multi-physics PDE simulation. In International Conference on Computational Science (ICCS2002) Workshop on PDE Software, April 21-24, 2002.
- Schniewind, A. P., Centeno, J.C. (1973) Fracture toughness and duration of load factor I. Six principal systems of crack propagation and the duration factor for cracks propagating parallel to grain. *Wood Fiber* 5:152-159
- Stanzl-Tschegg, S. E., Tan, D. M., Tschegg, E. K. (1995) New splitting method for wood fracture characterization. *Wood Science and Tech.* 29:31-50
- Sulsky, D., Chen, Z., Schreyer, H.L. (1994) A particle method for history-dependent materials. *Comput. Methods Appl. Mech. Engrg.* 118:179-186.
- Sulsky, D., Zhou, S.-J., Schreyer, H.L. (1995) Application of a particle-in-cell method to solid mechanics. *Comput. Phys. Commun.* 87:236-252
- Sulsky, D., Schreyer, H.L. (1996) Axisymmetric form of the material point method with applications to upsetting and Taylor impact problems. *Comput. Methods. Appl. Mech. Engrg.* 139:409-429
- Thuvander, F., Sjudahl, M., Berglund, L.A. (2000) Measurements of crack tip strain field in wood at the scale of growth rings. *Journal of Materials Science* 35:6267-6275.
- Thuvander, F., Berglund, L.A. (2000) In situ observations of fracture mechanisms for radial cracks in wood. *Journal of Materials Science* 35:6277-6283
- Zhou, S. (1998) *The Numerical Prediction of Material Failure Based on the Material Point Method*. PhD thesis, University of New Mexico

Submitted: September 8th 2006

Revised: October 17th 2006